Wei-Wen Yu International Specialty Conference on Cold-Formed Steel Structures
St. Louis, Missouri, U.S.A., November 7 & 8, 2018

Biaxial bending of cold-formed steel storage rack uprights - Part I: FEA and parametric studies

Nima Talebian[1], Benoit P. Gilbert[1], Cao Hung Pham[2], Romain Chariere[1] and Hassan Karampour[1]

Abstract

This paper first introduces an advanced finite element model to determine the biaxial bending capacity of cold-formed steel storage rack upright sections. The model is found to accurately predict published experimental results with an average predicted to experimental capacity ratio of 1.02. Second, the validated model is used to run parametric studies and analyse the biaxial response of slender, semi-compact and compact unperforated storage rack upright cross-sections. Analyses are run for local and distortional buckling failure modes only. Ten and four different cross-sectional shapes are analysed for local and distortional buckling, respectively, and nine biaxial bending configurations are considered per cross-section and buckling mode. Results show that a nonlinear interactive relationship typically governs the biaxial bending of the studied uprights. This relationship is discussed in some details and analysed for the different failure modes and cross-sectional slenderness.

Introduction

Rack-supported buildings, also referred to as “clad racks”, are gaining popularity. In this type of buildings, stored goods and building enclosure are both supported by the storage racks, resulting in more economical buildings but also complex structural systems. The uprights, i.e. the vertical members of the storage racks which are usually perforated monosymmetric open sections, undergo biaxial bending due to combined actions of wind loading and the vertical loads of the stored goods (Talebian et al. 2018). Current cold-formed steel structures design specifications (North American Specification AISI-S100 (AISI 2016), the Australian and New Zealand Standard AS/NZS 4600:2005 (AS/NZS 2005) and the Eurocode 3 EN1993-1-3 (CEN 2006)) consider a linear interaction equation to design members under biaxial bending. Nevertheless, previous studies have shown

[1] Griffith School of Engineering and Built Environment, Griffith University, Gold Coast, Australia
[2] School of Civil Engineering, The University of Sydney, Sydney, Australia

that a nonlinear relationship governs the biaxial bending behaviour of cold-formed steel members and the linear equation is conservative (Put et al. 1999; Torabian et al. 2016, 2014a, 2015; Talebian et al. 2018).

An experimental investigation on the local and distortional biaxial bending behaviour of cold-formed steel storage rack uprights (Talebian et al. 2018) has recently been performed at Griffith University, Australia. The investigation included tests on two different types of storage rack uprights. One of the upright sections was tested with and without regular perforations while the other one was perforated. Results showed that the linear interaction equation is conservative and underestimates the biaxial bending capacity by up to 68%.

As part of an ongoing research project, this paper presents an advanced Finite Element (FE) model to accurately capture the local and distortional biaxial bending capacities of cold-formed steel storage rack upright sections. The software package ABAQUS (2015) is used for this purpose and the experimental results in Talebian et al. (2018) are compared to the numerical ones to verify the accuracy of the FE model. The model is subsequently used to run parametric studies and quantify the local and distortional biaxial bending capacities of slender, semi-compact and compact unperforated storage rack upright cross-sections. Ten and four different cross-sections are considered for local and distortional buckling, respectively, and analyses are run for nine biaxial bending configurations per cross-section type and buckling mode. Biaxial bending responses of all studied uprights are discussed and presented in the paper.

Published experimental tests

Experimental set-up

In Talebian et al. (2018), two different types of storage rack upright cross-sections, referred to as “Type A” and “Type B”, were tested. Type A upright had a nominal wall thickness of 1.5 mm, a width-to-depth ratio of 0.71 and a semi-compact cross-sectional shape. Type B upright had a nominal wall thickness of 2.0 mm, a width-to-depth ratio of 0.5 and was compact. To investigate the effect of perforations on the member capacity and biaxial bending interaction, Type A uprights were tested with and without regular perforations along their length, whereas all tested Type B uprights were perforated. To ensure local and distortional buckling failure modes, the length of the uprights varied and was equal to 400 mm for local buckling, and 900 mm (Type B) and 1,100 mm (Type A) for distortional buckling. 10 mm thick, 220 mm × 220 mm steel plates were welded to both ends of the uprights to connect to the test rig and restrained warping. The full test rig is detailed in Talebian et al. (2018).

To obtain a sufficient number of points and apprehend the biaxial bending interaction curve, seven different biaxial bending configurations per upright type were tested in Talebian et al. (2018). These included bending about x-axis of symmetry (Conf 1), $M_x = 2M_y$ (Conf 2), $M_y = 2M_x$ (Conf 3), bending about minor y-axis when web is in compression (Conf 4), $M_x = -2M_y$ (Conf 5), $M_y = -2M_x$ (Conf 6) and bending about minor y-axis when flanges are in compression (Conf 7), where M_x and M_y are the moments applied about x- and y-axes, respectively. Tests were typically repeated twice for each configuration and upright type. In total, 78 tests were performed.

Geometric imperfection measurements

The structural performance of cold-formed members is highly sensitive to initial geometric imperfections (Dubina, et al., 2000, Schafer and Peköz, 1998). Accurately measuring these imperfections is essential to reproduce the observed buckling behaviour in FEA (Dubina and Ungureanu, 2002). Therefore, geometric imperfections of semi-compact Type A upright, with and without perforations, were measured prior to testing for all local and distortional specimens. As Type B upright had a compact cross-section, imperfections were not recorded.

An imperfection measurement set-up, similar to the one used by Schafer and Pekoz (1998), was built to capture imperfections along the upright length using Linear Variable Displacement Transducers (LVDT). Locations of LVDT were chosen to account for local and distortional buckling modes. In total, imperfections were measured along fifteen lines.

Finite element model

Element type, mesh size and boundary conditions

The uprights and end plates were modelled using S4R shell elements (ABAQUS, 2015). Convergence studies showed that an element size of approximately 3 mm x 3 mm was adequate for all cases. Similar boundary conditions as in the experimental tests were used: (i) warping was restrained by using end plates rigidly connected to the ends of the uprights, (ii) the uprights were simply supported by pinning the end plates at the location of the uprights centroidal axis. A concentrated biaxial bending moment was then applied at the pinned joints to replicate the test set-up. Figure 1 shows the FE model and boundary conditions for a 1,100 mm Type A upright. Note that only the main perforations were modelled for the perforated uprights.

Material modelling

Material non-linearity in the specimens was considered using with the von Mises yield criteria and isotropic hardening. The average coupon test results reported in

Talebian et al (2018) were used for the material properties of the flat parts of the cross-sections. The stress-strain relationships (derived from the coupon tests) were described by multi-linear curves, as showed in Figure 2 for all upright types. As the coupon material tests also measured the effect of residual stresses in the material, the membrane residual stresses were ignored in this model.

The enhanced yield ΔF_y stress in the corner zones of the upright sections was determined by the following equations (Karren,1967):

$$\Delta F_y = 0.6\left[\frac{B_c}{(r/t)^m} - 1.0\right]F_y \tag{1}$$

$$B_c = 3.69\left(\frac{F_u}{F_y}\right) - 0.819\left(\frac{F_u}{F_y}\right)^2 - 1.79 \tag{2}$$

$$m = 0.192\left(\frac{F_u}{F_y}\right) - 0.068 \tag{3}$$

where F_u is the ultimate strength, F_y the yield stress, r the inside bending radius of the corner and t the wall thickness. The corner zone consists of the curved areas and two equivalent flat areas on both sides of each curved area of length equal to 1/2πr. The measured thickness of the uprights was used to calculate the enhanced corner strength. The inside bending radius of the corners was 3 mm and 2 mm, for Type A and B uprights, respectively. An elastic–perfectly plastic behaviour was assumed for the corners with enhanced yield strength as per the stress-strain curves in Karren (1967).

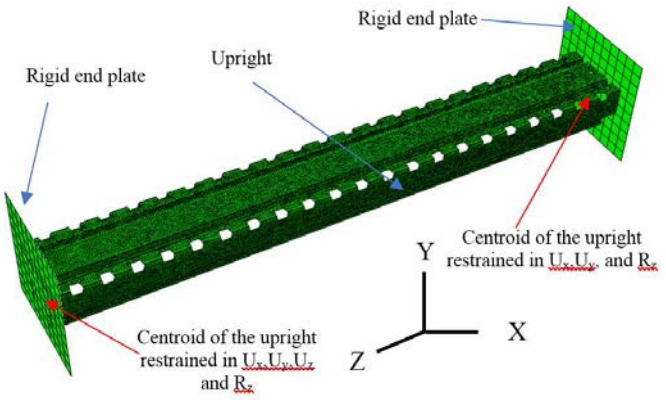

Figure 1. FE model and boundary conditions (shown for 1,100 mm perforated Type A upright)

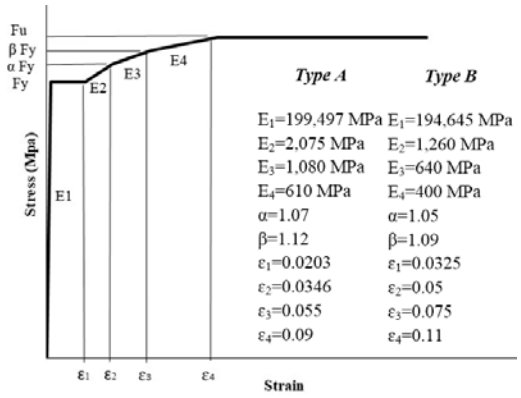

Figure 2. Multi-linear stress–strain curve adopted in the numerical simulations

To account for the change of cross-sectional dimensions of the coupons during testing, true engineering stress and strain were employed in the numerical model. The nominal stress (σ_n) and strain (ε_n) were converted to true stress (σ_t) and strain (ε_t) using the following equations (Chung and Ip, 2000):

$$\sigma_t = \sigma_n(1+\varepsilon_t) \tag{4}$$

$$\varepsilon_t = ln(1+\varepsilon_n) \tag{5}$$

Geometric imperfections

As mentioned earlier, imperfections were measured for semi-compact Type A upright. The readings collected by the data logger were smoothed using a Fourier Transform to filter the noise. The geometric imperfections at each measured line were then added to the "perfect" model assuming an undeformed cross-section at both ends of the uprights. Linear interpolations were assumed between each measured lines in the "imperfect" model.

For Type B upright, geometric imperfections were introduced in the model using axial compressive buckling modes. An initial linear buckling analysis (LBA) was carried out on a "perfect" model to generate the deformed shape of the local or distortional buckling modes. The geometric imperfections were then introduced to the "perfect" mesh by means of linearly superimposing the first local (for the 400 mm long specimens) or the first distortional (for the 900 mm and 1,100 mm long specimens) elastic buckling mode onto the mesh. The elastic buckling deformed shapes were scaled using the recommendations in the Australian standard AS4084 (2012). For the first local buckling mode, the following amplitude S_{ol} was used:

$$S_{ol} = 0.3t\sqrt{\left(\frac{F_y}{F_{ol}}\right)} \tag{6}$$

and for the first distortional buckling mode, the amplitude S_{od}:

$$S_{od} = 0.3t\sqrt{\left(\frac{F_y}{F_{od}}\right)} \tag{7}$$

where t is the thickness of the upright, F_y is the yield stress, F_{ol} the elastic local buckling stress and F_{od} the elastic distortional buckling stress.

Analysis

The arc-length method (Riks) was selected to perform geometric and material nonlinear analyses in ABAQUS.

Validation of FE model

Table 1 shows the ultimate test to predicted bending moment ratios (M_{test}/M_{FEA}) for the local and distortional buckling investigations and for all tested configurations. The table shows that the FE model is able to accurately predict the ultimate experimental moment capacities with a maximum difference between the predicted and experimental ultimate bending moment of 10%. The mean values of the test-to-predicted bending strength ratios are 0.98 and 1.03 for all local and distortional buckling tests, respectively, and the corresponding coefficient of variation (COV) are 5% and 5.8%, respectively.

Figure 3 to Figure 5 show the FEA and experimental failure modes of the 400 mm long uprights. Similarly, Figure 6 to Figure 8 show the FEA and experimental failure modes of the 900 mm and 1,100 mm long uprights. The FEA model is also able to well capture the different experimentally observed biaxial bending failure modes of the uprights.

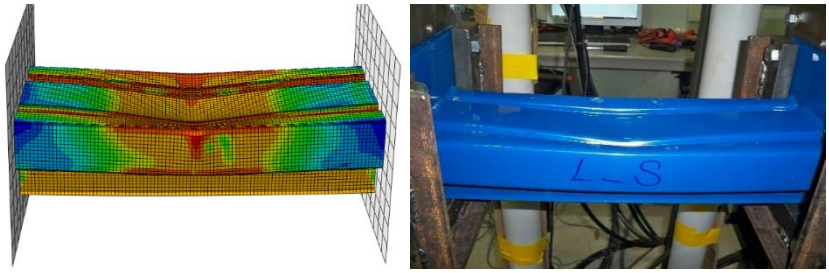

(a) (b)

Figure 3. Deformed shapes of the 400 mm long upright tested in Conf 4 for non-perforated Type A upright a) FE failure mode and b) experimental failure mode

Table 1. Comparison of test results with FEA results

Upright type	Local			Distortional		
	Number of tests	Conf.	(M_{test}/M_{FEA})	Number of tests	Conf.	(M_{test}/M_{FEA})
Non-perforated Type A	2	1	0.93	2	1	0.94
			0.93			0.98
	2	2	1.02	2	2	1.10
			1.02			1.03
	2	3	1.04	2	3	1.07
			1.00			1.10
	2	4	1.00	2	4	1.08
			0.98			1.05
	2	5	0.95	2	5	1.05
			0.94			1.07
	2	6	0.94	2	6	0.99
			0.94			0.93
	2	7	0.99	2	7	1.08
			1.01			1.10
Perforated Type A	2	1	0.90	2	1	0.99
			0.93			0.95
	2	2	0.97	2	2	1.08
			1.00			1.07
	2	3	1.01	2	3	1.1
			1.02			1.08
	2	4	1.00	2	4	1.09
			0.99			1.09
	2	5	0.93	2	5	1.07
			0.90			1.06
	2	6	0.94	2	6	0.9
			0.96			1.02
	2	7	1.00	2	7	1.08
			0.97			1.10
Perforated Type B	1	1	1.03	2	1	1.00
	1	2	0.96			0.95
	1	3	0.92	2	2	1.01
	1	4	1.03			0.96
	1	5	1.01	2	3	1.09
	2	6	1.10			1.01
	1	7	1.08	2	4	1.1
						0.99
				2	5	0.91
						0.94
				2	6	0.98
						0.98
				2	7	1.02
						1.04
		Average	0.98		Average	1.03
		COV (%)	5.00		COV (%)	5.80

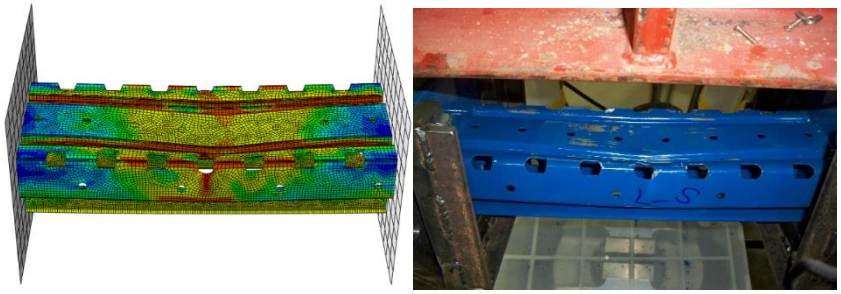

(a) (b)

Figure 4. Deformed shapes of the 400 mm long upright tested in Conf 3 for perforated Type A upright a) FE failure mode and b) experimental failure mode

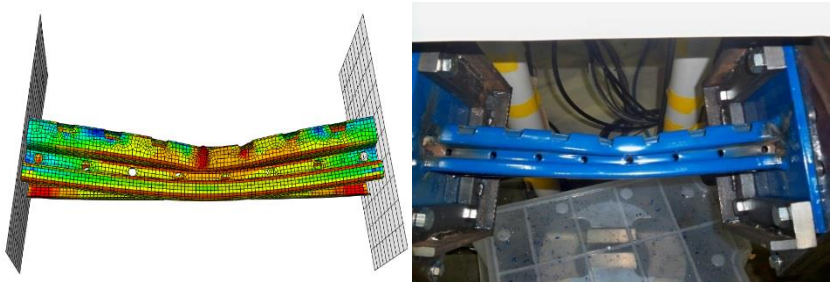

(a) (b)

Figure 5. Deformed shapes of the 400 mm long upright tested in Conf 2 for perforated Type B upright a) FE failure mode and b) experimental failure mode

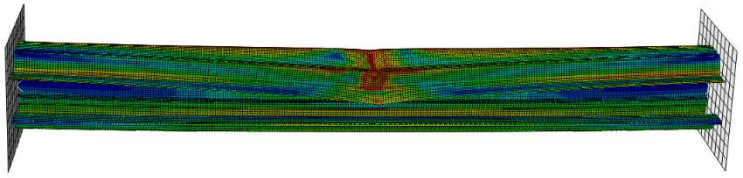

(a)

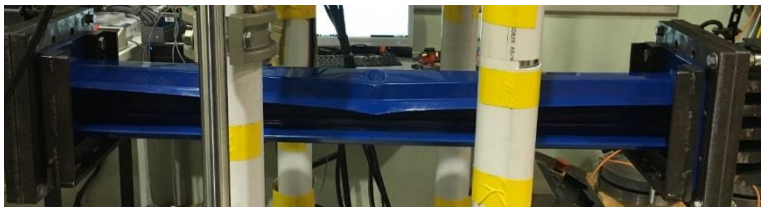

(b)

Figure 6. Deformed shapes of the 1,100 mm long upright tested in Conf 1 for non-perforated Type A upright a) FE failure mode and b) experimental failure mode

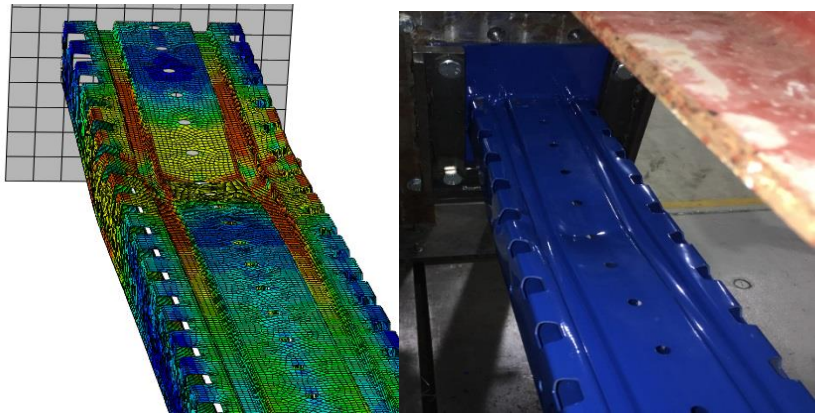

(a) (b)

Figure 7. Deformed shapes of the 1,100 mm long upright tested in Conf 4 for perforated Type A upright a) FE failure mode and b) experimental failure mode

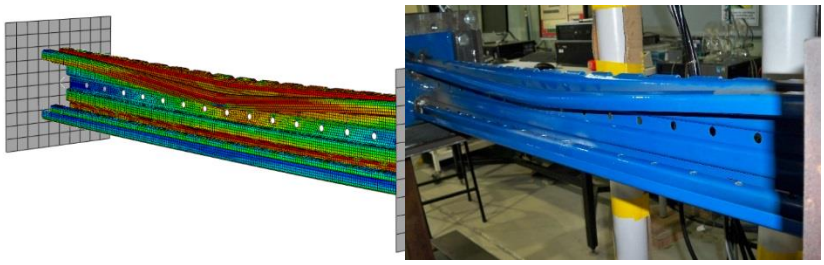

(a) (b)

Figure 8. Deformed shapes of the 9100 mm long upright tested in Conf 1 for perforated Type B upright a) FE failure mode and b) experimental failure mode

Parametric studies

Parametric studies are performed in this paper over a wider range of section slenderness values than the ones encountered in Talebian et al. (2018) to fully capture the biaxial bending behaviour of cold-formed steel storage rack uprights. Slender, semi-compact and compact unperforated upright cross-sections are considered for both local and distortional buckling failure modes. Note that unperforated uprights are considered for simplicity as experimental results in Talebian et al. (2018) tend to show that the biaxial bending behaviour of the uprights is not influenced by the regular perforations along their length.

Tested configurations and upright lengths

Ten and four upright cross-sectional shapes were investigated for local and distortional buckling failure modes, respectively. These upright cross-sectional shapes are shown in Figure 9 and are either commercially available or taken from the literature (Lau and Hancock, 1987; Bernuzzi and Simoncelli, 2015). In total, twelve different cross-sectional shapes are considered with Types D and F used for both local and distortional analyses. The thickness of Types J, K and L has been intentionally reduced to increase their slenderness ratio. The main cross-sectional dimensions and properties of all upright types are given in Table 2. Note that depending on the value of the biaxial moments, it is possible to have different range of slenderness ratio per upright type. In general, a section is considered to be slender when its slenderness ratio is greater than 1.25 (Martins et al. 2016).

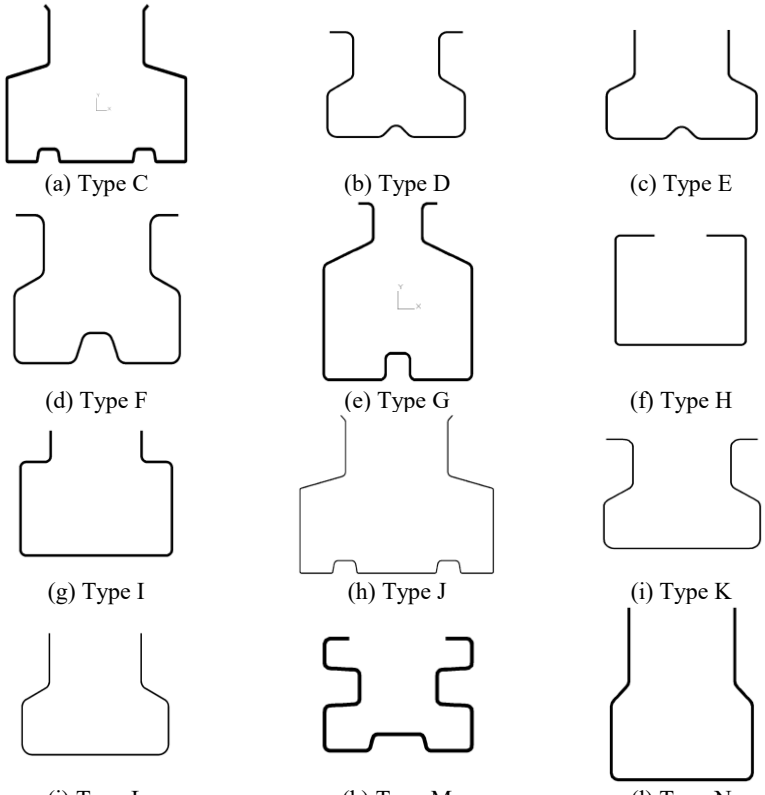

(a) Type C (b) Type D (c) Type E

(d) Type F (e) Type G (f) Type H

(g) Type I (h) Type J (i) Type K

(j) Type L (k) Type M (l) Type N

Figure 9. Upright cross-sections considered

Table 2. Nominal cross-sectional dimensions and properties of investigated uprights

	Thick. (mm)	Depth (mm)	Width (mm)	Second moment of area I_{Major} / I_{Minor}	Local buckling upright length (mm)	Dist. buckling upright length (mm)
Type C	2.0	140	100	2.53	200	--
Type D	1.2	90	72	1.58	120	860
Type E	1.2	90	72	2.06	120	--
Type F	1.5	125	100	1.79	200	1240
Type G	1.5	100	110	0.94	220	--
Type H	1.5	100	90	1.41	350	--
Type I	1.5	100	80	2.13	240	--
Type J	0.6	140	100	2.53	300	--
Type K	0.8	90	72	1.57	200	--
Type L	0.8	90	72	2.03	260	--
Type M	1.8	80	60	2.17	--	800
Type N	1.5	80	90	1.17	--	600

Nine biaxial bending configurations, shown in Table 3, were considered per buckling mode and upright type. The numerical analyses were run using similar models to the ones presented in Section "Finite Element model". Characteristics specific to the parametric studies and used in the present models are given later in Section "Modelling characteristics".

The length of the tested uprights were determined based on elastic buckling analyses performed in CUFSM (2006) with simply supported and free-to-warp beams. For local buckling, the upright length for each upright type was taken as four times the longest local buckling half-wave length of the nine biaxial bending configurations. This criterion ensured that the uprights were short enough so distortional buckling did not occurred. For distortional buckling, the upright length for each upright type was taken equal to 1 to 2 times the longest distortional buckling half-wave length of the nine investigated configurations, effectively preventing global buckling. To avoid local-distortional buckling interaction to occur, LBA were carried out in ABAQUS on the warping restrained beams for all nine biaxial bending configurations. Any configuration for which the ratio of the elastic local bending moment (M_{ol}) to the elastic distortional bending moment (M_{od}) was less than 1.3 (Martins et al., 2016) was excluded from the analyses. The lengths of all uprights are given in Table 2.

Modelling characteristics

In the parametric studies, the stress-strain curve of the flat parts of the upright sections used in all analyses is similar to the one for Type A presented in Figure 2, but with a Young's modulus of 200 GPa and a yield stress of 450 MPa. An elastic-perfectly plastic material is also used for the corner zones with the yield stress calculated from Eqs. 3-5.

Table 3. Tested biaxial bending configurations in parametric studies

Configuration 0	*Configuration 1*	*Configuration 2*
$M_x > 0$ and $M_y = 0$	$M_x > 0$, $M_y > 0$ and $M_x = 2.5M_y$	$M_x > 0$, $M_y > 0$ and $M_x = M_y$
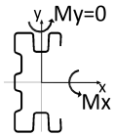	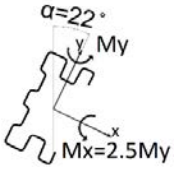	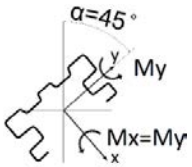
Configuration 3	*Configuration 4*	*Configuration 5*
$M_x > 0$, $M_y > 0$ and $M_y = 2.5M_x$	$M_x = 0$ and $M_y > 0$	$M_x > 0$, $M_y < 0$ and $M_x = -2.5M_y$
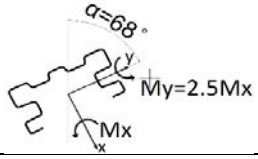	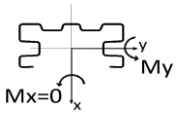	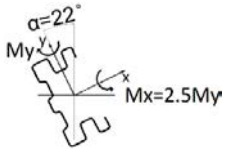
Configuration 6	*Configuration 7*	*Configuration 8*
$M_x > 0$, $M_y < 0$ and $M_x = -M_y$	$M_x > 0$, $M_y < 0$ and $M_y = -2.5M_x$	$M_x = 0$ and $M_y < 0$
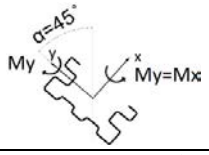	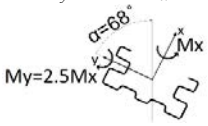	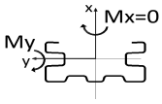

$M_x > 0$ generates compression in the bottom flange, $M_y > 0$ generates compression in the lip stiffeners and $M_y < 0$ generates compression in the web

Geometric imperfections are introduced in the analyses following the methodology described in Section "Geometric imperfections" for Type B upright. In other words, the first local or distortional buckling mode deformed shape in pure compression is used and scaled by the factors obtained from Eqs. 6-7.

Biaxial bending response of the uprights and interactive behaviour

Local buckling

Elastic and inelastic local buckling failure modes were observed for all specimens investigated for local buckling. Denoting, the bending moment capacities about the x- and y-axes, M_{bx} and M_{by}, respectively, the normalised biaxial ultimate moment capacities (M_x/M_{bx} and M_y/M_{by}) for all upright types are summarised in Table 4 with local slenderness ratio λ_l (determined from FE model running LBA)

and the associated interactive biaxial moment capacity obtained from the linear equation (AISI-S100, 2016; AS/NZS 4600:2005; EN 1993-1-3, 2006). Figure 10 illustrates differently the linear equation versus the normalised biaxial bending results obtained from the nine different investigated configurations and local buckling. Similar observations to the ones presented in Talebian et al. (2018), but on a larger range of cross-sections can be established. Table 4 and Figure 10 show that the governing interaction relationship is not linear and that the linear equation is conservative for all investigated uprights. For Configurations 1 to 3 ($M_y > 0$, lip stiffeners in compression), the linear equation gives interaction ratios ranging from 1.12 (Type H and Configuration 1) to 1.35 (Type L and Configuration 1). For Configurations 5 to 7 ($M_y < 0$, web in compression), the linear equation gives ratios ranging from 1.03 (Type L and Configuration 7) to 1.39 (Type E and Configurations 5 and 6). When the web is in compression, the biaxial bending responses of the uprights tend to be closer to the linear interaction curve. This is more highlighted for Type K and L uprights.

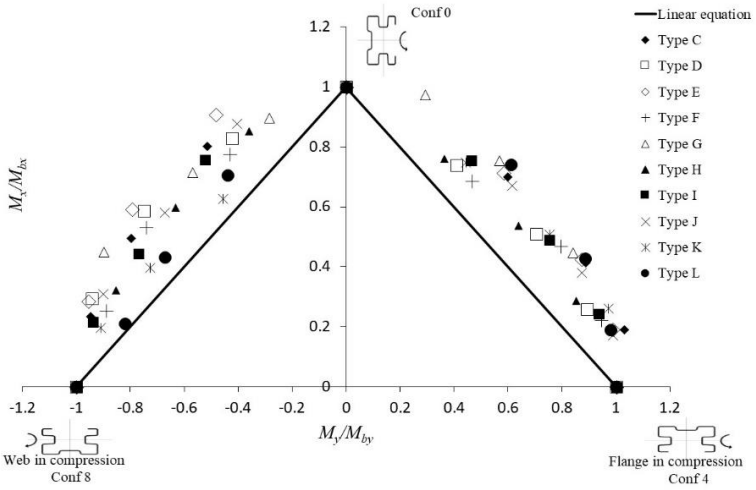

Figure 10. Biaxial bending interaction points for local buckling – All uprights

Distortional buckling

For distortional buckling analyses, Type D, E and M uprights tested with the web in compression (Configurations 5 to 8) did not meet the M_{ol} /M_{od} ratio less than 1.3 (Martins et al., 2016) and would have failed in local or local-distortional buckling interaction. Therefore, these configurations were excluded from the analyses. The normalised ultimate moment capacities (M_x/M_{bx} and M_y/M_{by}) for the upright types considered for distortional buckling are summarised in Table 5 with

distortional slenderness ratio λ_d (also determined from LBA in Abaqus) and the interactive biaxial moment linear equation. Similar to Figure 10, Figure 11 illustrates the linear interaction equation versus all normalised biaxial bending numerical results obtained for distortional buckling failure modes.

The linear equation is also found to be conservative for distortional buckling and gives interaction ratios ranging from 1.00 (Type F and Configuration 1) to 1.46 (Type N and Configuration 2) for all biaxial bending configurations. Biaxial bending responses of Type F upright tend to be closer to the linear interaction curve than other uprights.

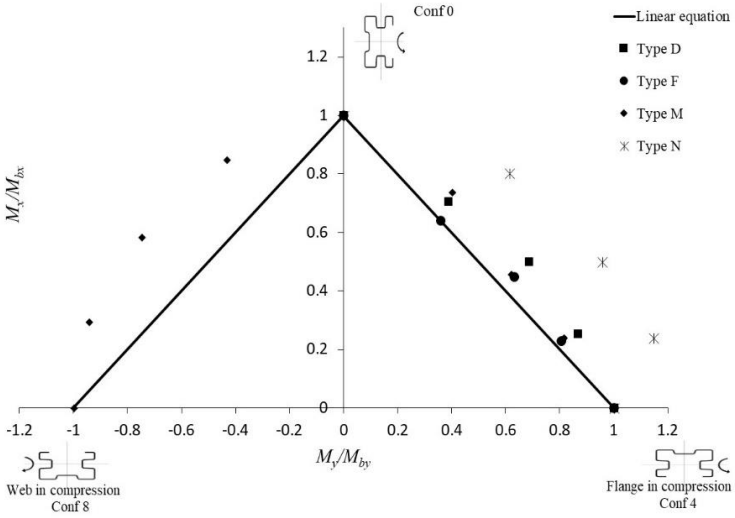

Figure 11. Biaxial bending interaction points for distortional buckling – All uprights

Conclusion

This paper presented a FE model to capture the biaxial bending response of cold-formed steel storage rack uprights. The model was validated against experimental results and found to be accurate. Parametric studies were then performed to evaluate the accuracy of the linear biaxial bending design equation in international design specifications (AISI-S100 (2016), AS/NZS 4600:2005 (AS/NZS, 2005) and EN 1993-1-3 (2006)). Analyses were performed for local and distortional buckling failure modes only. The biaxial bending interaction relationship was found to be nonlinear and the linear biaxial bending design equation to be conservative with failure occurring at ratios given by the design equation ranging from 1.00 to 1.46.

Table 4. Comparison of parametric studies results to linear equation for local buckling

Up-right	Conf.	λ_l	M_x/M_{bx}	M_y/M_{by}	Linear equation	Up-right	Conf.	λ_l	M_x/M_{bx}	M_y/M_{by}	Linear equation
Type C	0	0.57	1.00	0.00	1.00	Type H	0	1.30	1.00	0.00	1.00
	1	0.78	0.70	0.60	1.30		1	1.17	0.76	0.36	1.12
	2	0.83	0.42	0.89	1.30		2	1.08	0.54	0.64	1.18
	3	0.74	0.19	1.03	1.22		3	1.03	0.29	0.85	1.14
	4	0.71	0.00	1.00	1.00		4	1.06	0.00	1.00	1.00
	5	0.52	0.80	0.52	1.32		5	1.06	0.85	0.36	1.22
	6	0.43	0.50	0.80	1.30		6	1.01	0.60	0.63	1.23
	7	0.40	0.24	0.95	1.19		7	1.09	0.32	0.86	1.18
	8	0.41	0.00	1.00	1.00		8	1.23	0.00	1.00	1.00
Type D	0	0.58	1.00	0.00	1.00	Type I	0	0.83	1.00	0.00	1.00
	1	0.61	0.74	0.41	1.15		1	0.72	0.76	0.46	1.22
	2	0.62	0.51	0.70	1.21		2	0.72	0.49	0.75	1.24
	3	0.60	0.26	0.89	1.15		3	0.64	0.24	0.94	1.18
	4	0.61	0.00	1.00	1.00		4	0.62	0.00	1.00	1.00
	5	0.47	0.83	0.42	1.25		5	0.90	0.76	0.52	1.28
	6	0.46	0.59	0.75	1.34		6	1.02	0.45	0.77	1.22
	7	0.44	0.29	0.94	1.24		7	0.98	0.22	0.94	1.16
	8	0.45	0.00	1.00	1.00		8	1.01	0.00	1.00	1.00
Type E	0	0.90	1.00	0.00	1.00	Type J	0	1.88	1.00	0.00	1.00
	1	1.19	0.71	0.58	1.30		1	1.65	0.67	0.61	1.29
	2	1.30	0.43	0.87	1.30		2	1.74	0.38	0.87	1.25
	3	1.08	0.19	0.99	1.18		3	1.54	0.17	0.99	1.16
	4	1.05	0.00	1.00	1.00		4	1.48	0.00	1.00	1.00
	5	0.52	0.91	0.48	1.39		5	1.71	0.88	0.41	1.29
	6	0.48	0.59	0.79	1.39		6	1.39	0.58	0.68	1.26
	7	0.42	0.29	0.96	1.24		7	1.29	0.31	0.90	1.21
	8	0.39	0.00	1.00	1.00		8	1.30	0.00	1.00	1.00
Type F	0	0.64	1.00	0.00	1.00	Type K	0	0.88	1.00	0.00	1.00
	1	0.71	0.69	0.47	1.15		1	0.91	0.75	0.44	1.19
	2	0.69	0.47	0.80	1.26		2	0.90	0.51	0.75	1.26
	3	0.66	0.22	0.94	1.17		3	0.87	0.26	0.97	1.23
	4	0.68	0.00	1.00	1.00		4	0.89	0.00	1.00	1.00
	5	0.58	0.78	0.43	1.21		5	1.18	0.63	0.46	1.09
	6	0.52	0.53	0.74	1.28		6	1.36	0.40	0.73	1.13
	7	0.47	0.26	0.89	1.15		7	1.47	0.20	0.91	1.11
	8	0.47	0.00	1.00	1.00		8	1.65	0.00	1.00	1.00
Type G	0	1.03	1.00	0.00	1.00	Type L	0	1.43	1.00	0.00	1.00
	1	0.87	0.98	0.29	1.27		1	1.89	0.74	0.61	1.35
	2	0.72	0.76	0.57	1.32		2	1.90	0.43	0.89	1.31
	3	0.50	0.45	0.84	1.29		3	1.72	0.19	0.98	1.17
	4	0.42	0.00	1.00	1.00		4	1.68	0.00	1.00	1.00
	5	0.92	0.90	0.29	1.18		5	1.31	0.71	0.44	1.14
	6	0.84	0.72	0.57	1.29		6	1.45	0.43	0.67	1.10
	7	0.67	0.45	0.90	1.35		7	1.41	0.21	0.82	1.03
	8	0.52	0.00	1.00	1.00		8	1.46	0.00	1.00	1.00

Table 5. Comparison of parametric studies results with linear equation for distortional buckling

Up-right	Conf.	λ_d	M_x/M_{bx}	M_y/M_{by}	Linear equation	Up-right	Conf.	λ_d	M_x/M_{bx}	M_y/M_{by}	Linear equation
Type D	0	0.74	1.00	0.00	1.00	Type F	0	0.78	1.00	0.00	1.00
	1	0.76	0.71	0.39	1.09		1	0.83	0.64	0.36	1.00
	2	0.76	0.50	0.69	1.18		2	0.80	0.45	0.63	1.08
	3	0.72	0.25	0.87	1.12		3	0.75	0.23	0.81	1.03
	4	0.74	0.00	1.00	1.00		4	0.77	0.00	1.00	1.00
Type M	0	0.63	1.00	0.00	1.00	Type N	0	1.29	1.00	0.00	1.00
	1	0.66	0.74	0.40	1.14		1	1.39	0.80	0.61	1.42
	2	0.63	0.46	0.62	1.08		2	1.32	0.50	0.96	1.46
	3	0.57	0.24	0.81	1.05		3	1.26	0.24	1.15	1.39
	4	0.59	0.00	1.00	1.00		4	1.25	0.00	1.00	1.00
	5	0.36	0.85	0.43	1.28						
	6	0.31	0.59	0.75	1.33						
	7	0.30	0.30	0.94	1.24						
	8	0.33	0.00	1.00	1.00						

References

Abaqus (2015). "Abaquas ver 6.14 user manual " Providence, U.S.A.: ABAQUS, Inc.

AS/NZS (2005). *Cold-formed steel structures*, Sydney: Australia: Standards Australia.

AS4084, *Steel storage racking*. 2012, Sydney, Australia: Standards Australia.

AISI-S100 (2016). "North American Specification for the design of cold-formed steel structural members." *American Iron and Steel Institute*.

Bernuzzi, C., and Simoncelli, M. (2015). "European design approaches for isolated cold-formed thin-walled beam–columns with mono-symmetric cross-section." *Engineering Structures,* 86: p. 225-241.

Chung, K. F., and Ip, K. H. (2000) . "Finite element modeling of bolted connections between cold-formed steel strips and hot rolled steel plates under static shear loading." *Engineering Structures*, 22(10): p. 1271-1284.

Dubina, D., and Ungureanu, V. (2002). "Effect of imperfections on numerical simulation of instability behaviour of cold-formed steel members." *Thin-Walled Structures*, 40(3), 239-262.

Dubina, D., Ungureanu, V., and Szabo, I. (2000). "Influence of local and sectional geometrical imperfections on the distortional and interactive overall buckling modes of cold-formed members." *Proc., Proceedings of the 3rd International Conference on Coupled Instabilities in Metal Structures CIMS*, 179-188.

EN 1993-1-3 (2006). "Eurocode 3. Design of steel structures. General rules. Supplementary rules for cold-formed members and sheeting." European commitee for standardisation, Brussels, Belgium.

Karren, K. W. (1967). "Corner properties of cold-formed steel shapes." *Journal of Structural engineering*, 93(1), 401-432.
Lau, S.C.W., and Hancock, G.J. (1987). "Distortional buckling formulas for channel columns *Journal of Structural engineering*, 113(5), 1063-1078
Martins, A. D., Camotim, D., and Dinis, P. B. (2016). "On the direct strength design of cold-formed steel columns failing in local-distortional interactive modes" in *International Speciality Conference on Cold-Formed Steel Structures*, p. 135–153.
Put, B. M., Pi, Y.L., and Trahair, N. (1999). "Biaxial bending of cold-formed Z-beams." *Journal of Structural Engineering*, 125(11), 1284-1290.
Talebian, N., Gilbert, B.P., Pham, C.H., Chariere, R., and Karampour, H. (2018). "Local and distortional biaxial bending capacities of cold-formed steel storage rack uprights." *Journal of Structural Engineering*, 144(6).
Torabian, S., Fratamico, D. C., and Schafer, B. W. (2016). "Experimental response of cold-formed steel Zee-section beam-columns." *Thin-Walled Structures*, 98, 496-517.
Torabian, S., Zheng, B., and Schafer, B. (2014b). "Experimental study and modeling of cold-formed steel lipped channel stub beam-columns." *Proceedings of the Annual Stability Conference, Structural Stability Research Council, Toronto, Canada*.
Torabian, S., Zheng, B., and Schafer, B. W. (2014a). "Development of a new beam-column design method for cold-formed steel lipped channel members." *22nd international specialty conference on cold-formed steel design and construction*, 359-376.
Torabian, S., Zheng, B., and Schafer, B. W. (2015). "Experimental response of cold-formed steel lipped channel beam-columns." *Thin-Walled Structures*, 89, 152-168.
Schafer, B., and Peköz, T. (1998). "Computational modeling of cold-formed steel: characterizing geometric imperfections and residual stresses." *Journal of Constructional Steel Research*, 47(3), 193-210.